Viscoelastic Properties of f-actin, Microtubules, f-actin/α-actinin, and f-actin/Hexokinase Determined in Microliter Volumes with a Novel Nondestructive Method

O. Wagner,* J. Zinke,*# P. Dancker,¶ W. Grill,§ and J. Bereiter-Hahn*

*Zoologisches and #Physikalisches Institut der Johann Wolfgang Goethe Universität-Frankfurt/M, Frankfurt/M; §Fakultät für Physik und Geowissenschaften, Institut für Experimentalphysik II, Universität Leipzig, Leipzig; and ¶Institut für Zoologie der Technischen Universität Darmstadt, Darmstadt, Germany

ABSTRACT A nondestructive method to determine viscoelastic properties of gels and fluids involves an oscillating glass fiber serving as a sensor for the viscosity of the surrounding fluid. Extremely small displacements (typically 1–100 nm) are caused by the glass rod oscillating at its resonance frequency. These displacements are analyzed using a phase-sensitive acoustic microscope. Alterations of the elastic modulus of a fluid or gel change the propagation speed of a longitudinal acoustic wave. The system allows to study quantities as small as 10 μl with temporal resolution $>$1 Hz. For 2–100 μM f-actin gels a final viscosity of 1.3–9.4 mPa s and a final elastic modulus of 2.229–2.254 GPa (corresponding to 1493–1501 m/s sound velocity) have been determined. For 10- to 100-μM microtubule gels (native, without stabilization by taxol), a final viscosity of 1.5–124 mPa s and a final elastic modulus of 2.288–2.547 GPa ($\cong$1513–1596 m/s) have been determined. During polymerization the sound velocity in low-concentration actin solutions increased up to +1.3 m/s ($\cong$1.69 kPa) and decreased up to −7 m/s ($\cong$49 kPa) at high actin concentrations. On polymerization of tubulin a concentration-dependent decrease of sound velocity was observed, too (+48 to −12 m/s $\cong$ 2.3–0.1 MPa, for 10- to 100-μM tubulin). This decrease was interpreted by a nematic phase transition of the actin filaments and microtubules with increasing concentration. 2 mM ATP (when compared to 0.2 mM ATP) increased polymerization rate, final viscosity and elastic modulus of f-actin (17 μM). The actin-binding glycolytic enzyme hexokinase also accelerated the polymerization rate and final viscosity but elastic modulus (2.26 GPa) was less than for f-actin polymerized in presence of 0.2 mM ATP (2.28 GPa).

INTRODUCTION

Local mechanical properties of cytoplasm control cell shape and the direction of locomotion (Lüers and Bereiter-Hahn, 1992; Bereiter-Hahn and Lüers, 1998). Increasing evidence is brought forward for a subtle interplay between cell shape, invasiveness of tumor cells, the cytoskeletal organization, and gene expression (Emerman and Pitelka, 1977; Ingber, 1993; Bereiter-Hahn, 1994). In addition, the organization of a series of metabolic pathways by cytoskeletal structures has been reported (Bereiter-Hahn, 1997). Acoustic microscopy is among the few methods that allow study of the mechanical properties of cells (Bereiter-Hahn, 1995; Bereiter-Hahn et al., 1995). This might bridge the gap between the level of supramolecular structures and ultrasound signals used in medical diagnosis.

Cellular mechanics depends on the properties of the three major protein polymers, actin filaments, microtubules, and intermediate filaments, and their interactions with associated proteins (e.g., cross-linking proteins). Therefore, a method has been developed which allows synchronous determination of the acoustical and rheological parameters of cytogels (Kojro et al., 1996). The oscillating rod rheometer (ORR) simultaneously allows calculation of the volume elasticity of a fluid or gel from measurements of the velocity of longitudinal ultrasonic waves and determination of the dynamic viscosity from the oscillations (in a nanometer range) of a glass rod immersed in the viscous fluid. Compressibility of protein solutions reveals packing density and phase transitions (e.g., from liquid to liquid-crystal) and also conformational changes (Suzuki et al., 1996; Tamura et al., 1993; Leung et al., 1986). Therefore, determinations of the compression modulus are methods supplementary to nuclear magnetic resonance (NMR) spectroscopy and fluorescence resonance energy transfer (FRET).

In comparison to other rheometers (e.g., plate-plate or plate-cone rheometer), the oscillation of a glass rod acting as a sensor for viscosity causes a shear wave that is equivalent to the dimension of the rod and thus can propagate its full extent through the surrounding fluid with extremely small strain. This setup results in a more precise determination of the dynamic viscosity than that obtained by most other methods. Because stepwise changes of the oscillation amplitudes of the sensor are also possible, reversible and irreversible disruptions can be determined to analyze complex viscoelastic properties.

The system allows to study quantities as small as 10 μl with temporal resolution $>$1 Hz. Because the device has not been sealed during the measurement, the "online" addition of substances is possible.

The parameters derived from the ORR measurements are the time course of the dynamic viscosity and sound velocity,

Received for publication 27 July 1998 and in final form 12 February 1999.

Address reprint requests to Dr. J. Bereiter-Hahn, Biozentrum, AK Kinem. Zellforschung, Marie-Curie-Strasse 9, 60439 Frankfurt/M, Germany. Tel.: 49-69-7982-9608; Fax: 49-69-7982-9607; E-mail: bereiter-hahn@zoology.unifrankfurt.de.

0006-3495/99/05/2784/13 $2.00

e.g., during the polymerization of g-actin and tubulin under different conditions. The latter is equivalent to Young's elastic modulus E (at 1 GHz), which is not comparable to the dynamic storage modulus G′.

MATERIALS AND METHODS

Reagents

G-actin buffer: 2 mM TRIS-HCl (pH 7.4), 0.2 mM ATP, 0.5 mM DTT and 0.2 mM $CaCl_2$.

Polymerization buffer: 50 mM KCl and 2 mM $MgCl_2$.

Microtubule buffer: 80 mM PIPES-NaOH (pH 6.7), 1 mM GTP, 1 mM $MgCl_2$, 1 mM EGTA and 1 mM DTT.

Hexokinase buffer: 2 mM TRIS-HCl (pH 7.6), 2 mM or 0.2 mM ATP (depending on the assay), 0.5 mM DTT, 0.2 mM $CaCl_2$ and 1 mM PMSF.

Phalloidin, D-glucose, ATP-disodium salt and GTP-sodium salt were obtained from Sigma-Aldrich Chemie GmbH (Steinheim, Germany).

Proteins

G-actin was isolated from rabbit skeletal muscle (Spudich and Watt, 1971). α-actinin was prepared from chicken gizzard according to Feramisco and Burridge (1980). Polycycled tubulin (three times cycled, microtubule-associated protein-free and glycerol-free) was a generous gift from Dr. Müller-Reichert (EMBL-Institut, Heidelberg). It was prepared according to the method of Ashford and Hyman (1998). Hexokinase Type I from bovine heart (EC 2.7.1.1) was obtained from Sigma-Aldrich Chemie GmbH. The protein concentrations were determined according to the method of Bradford (1976). Prior to rheological measurements, protein solutions were degassed in vacuum for 10 min to avoid air bubbles, which otherwise strongly influence the measurements. Sample volume was 80–120 μl.

Electron microscopy

Actin filaments on glow-discharged carbon films were negatively stained with 1% uranyl acetate in water (Cooper and Pollard, 1982) and examined with a Zeiss 902 transmission electron microscope (Zeiss, Jena, Germany). Digital images were acquired via a CCD-Camera connected to the frame-grabbing and contrast enhancement device Argus-20 (Hamamatsu Photonics, Herrsching, Germany) and further processed with the HPD-CPx device control program (Hamamatsu Photonics, V.1.2).

The oscillating rod rheometer (ORR)

A glass fiber rod (diameter $\approx$ 50 μm, length $\approx$ 2 mm) was immersed in the fluid probe and stimulated to transversal oscillations (about 1–4 kHz, depending on the viscosity of the fluid and the length of the fiber) via a piezomechanical bimorph actuator (Fig. 1). The resonance frequency of the rod oscillation is, among other values (e.g., the density of the specimen), a function of the viscosity of the surrounding fluid. The extremely small displacements (>1 nm) of the rod are monitored by an acoustic microscope with phase-sensitive detection (Grill et al., 1996; Hillmann et al., 1994). High frequency pulses (1 GHz) are converted by a transducer into longitudinal acoustic waves, coupling into a sapphire and focused onto the free tip of the glass fiber. A circulating switch directs the high frequency pulses either to the acoustic lens or the detected signal to amplification and filtering components. A boxcar-integrator averages the received ultrasound pulses and filters undesirable interfering signals such as lens echoes.

The oscillation frequency of the rod is held at its resonance frequency via a feedback control: the phase of the rod oscillation is permanently compared with the phase of the piezo excitation frequency and is kept to a phase shift of $\pi/2$ by frequency adjustments. This function is accomplished by using a lock-in amplifier (model SR810, Stanford Research System Inc., Sunnyvale, CA) which also feeds the mean of the resonance frequency during one second into a PC (Fig. 2).

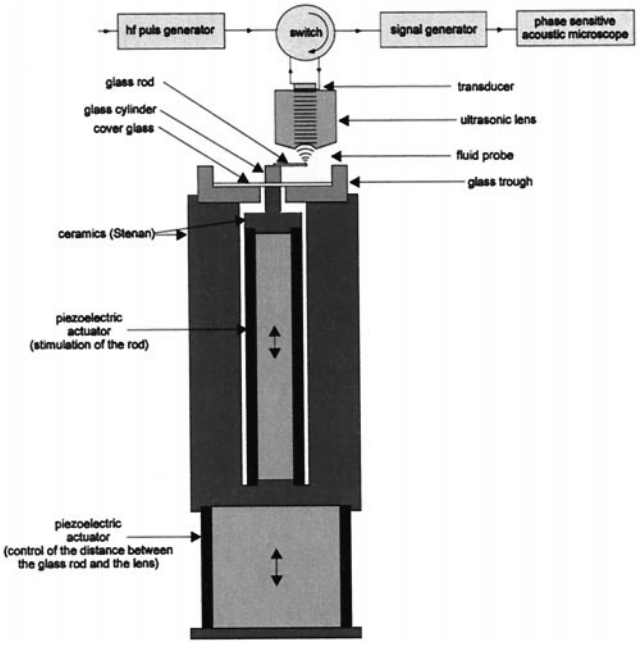

FIGURE 1 Diagrammatic view of the ORR. A glass fiber rod is immersed in the sample fluid and is stimulated to oscillate via piezoelectric actuator. The rod oscillation and the density of the specimen is a function of the dynamic viscosity of the surrounding fluid. The very small displacements (>1 nm) of the rod, are detected by an acoustic microscope with phase sensitive detection.

Changes of the propagation speed of the longitudinal acoustic waves in the sample shift the phase difference between the reflected ultrasound wave and the generating 1-GHz electric oscillation (e.g., the detected ultrasound signal is delayed when the sound velocity decreases). This phase shift is compensated by regulating the distance between the acoustic lens and the free tip of the glass fiber via a second piezoelectric actuator (Fig. 1). The voltage controlling this piezo actuator is a measure for the change of sound velocity, which is related to the volume elasticity of the probe (Eqs. 11 and 12).

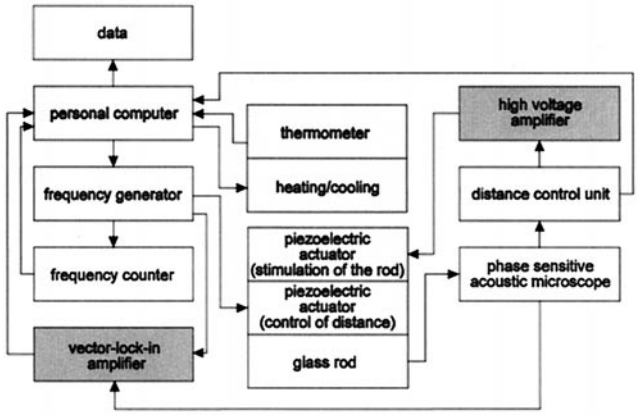

FIGURE 2 Block diagram of the entire setup.

Calculation of the viscosity (adapted from Kojro et al., 1996)

The actual oscillation of the rod stimulated externally at the fixed end with an amplitude (A) and the frequency (ω_A) is determined by the inertia force, the friction force and the resistance force:

$$\begin{array}{ccccccc} M\cdot\ddot{x} & + & R\cdot\dot{x} & + & k\cdot x & = & A\cdot\cos(\omega_A t) \\ \text{inertia force} & + & \text{friction force} & + & \text{resistance force} & = & \text{external force} \end{array} \quad (1)$$

where x is the displacement of the rod, M the effective mass of the rod (mass drag included), R the friction constant, k the elastic constant, A the amplitude of the external force, and ω_A the excitation frequency.

The effective mass M of the rod and the friction constant R are given by:

$$M = m_g + \rho(a + b\delta + c\delta^2) \quad (2)$$

and

$$R = \rho b' \delta \omega_A \quad (3)$$

where

$$\delta = \sqrt{\frac{2\eta}{\rho\omega}} \quad (4)$$

is the penetration depth of the shear wave (Lamb, 1932; Landau and Lifshitz, 1987) in a liquid (Fig. 3), η is the dynamic viscosity of the liquid, ρ is the density of the liquid, m_g the mass of the rod (without adhering liquid) and a, b, b′, and c are geometric constants.

It is obvious that the oscillating mass of the rod increases with the dimension of the induced viscous shear wave. This can be described as a mass drag effect (Fig. 3).

The solution of the differential equation (Eq. 1) is

$$x(t) = a(\omega)\cos(\omega t - \varphi(\omega)) \quad (5)$$

where $a(\omega)$ is the amplitude of the rod oscillations and $\varphi(\omega)$ is the phase shift between the excitation frequency and the frequency of the rod oscillation.

With Eqs. 1 and 5 we obtain the phase law described by Kojro et al. (1996):

$$\frac{\left(\frac{\omega_0^2}{\omega_A^2}\right) - 1}{\rho} = \alpha + \left(\beta + \frac{\beta'}{\tan\varphi}\right)\delta + \gamma\delta^2 \quad (6)$$

where ω_0 is the resonance frequency of the rod in vacuum (approximate in air) and α, β, β', and γ are constants of the apparatus.

Finally, the dynamic viscosity η (in mPa s, where 1 mPa s is 0.01 poise = 1 cP) is given by:

$$\eta = \left(\frac{\left(\beta + \frac{\beta'}{\tan\varphi}\right)\sqrt{\frac{\omega_A\rho}{8}}}{\gamma} + \sqrt{\frac{\left(\beta + \frac{\beta'}{\tan\varphi}\right)^2 \omega_A\rho}{8\gamma^2} + \left(\frac{\omega_0^2}{\omega_A^2} - 1\right)\frac{\omega_A}{2\gamma} - \frac{\alpha\omega_A\rho}{2\gamma}} \right)^2 \quad (7)$$

The constants α, β, β', and γ are derived from the determinations of the resonance frequencies in water-glycerol mixtures (0%, 5%, 10%, . . . 60%) of known viscosities determined with a commercial micro falling ball viscosimeter (HAAKE Mess-Technik, Karlsruhe, Germany). According to the phase law (Eq. 6), these data are then plotted with $(\omega_0^2/\omega^2 - 1)/\rho$ against $(2\eta/\rho\omega)$ (the square of the penetration depth of the shear wave in a liquid).

Calculation of the sound velocity and the elastic modulus

Acoustic waves are density oscillations in fluids or solids. In this experiment, the sound velocity (e.g., of water at 26°C of 1500 m/s, Kroebel and Mahrt, 1976) is related to the wavelength of the longitudinal acoustic wave (λ) and the operating frequency of the acoustic lens (ν):

$$c_{liquid} = \lambda\cdot\nu = 1.5\ \mu m\cdot 1\ GHz = 1500\ m/s \quad (8)$$

As mentioned before, the change of propagation speed of the acoustic wave can be compensated by a change of the distance (Δz) between the acoustic lens and the free tip of the glass fiber. This allows modification of Eq. 8 to:

$$c_{liquid} = (n\cdot\lambda_0 + \Delta z)\cdot\nu = (k\cdot V_{piezo})\cdot\nu \quad (9)$$

where k is a calibration constant determined for water = $c_{aqua}/V_{piezo}\cdot\nu$.

The compression modulus (volume elasticity), K, corresponds to the sound velocity, c, with:

$$c = \sqrt{\frac{K + \frac{4}{3}\cdot G}{\rho}} \quad (10)$$

where G is the shear modulus and ρ is the density of the liquid in g/cm^3.

Commonly $G \ll K$; therefore, Eq. 10 is approximated to:

$$c = \sqrt{\frac{K}{\rho}} \quad (11)$$

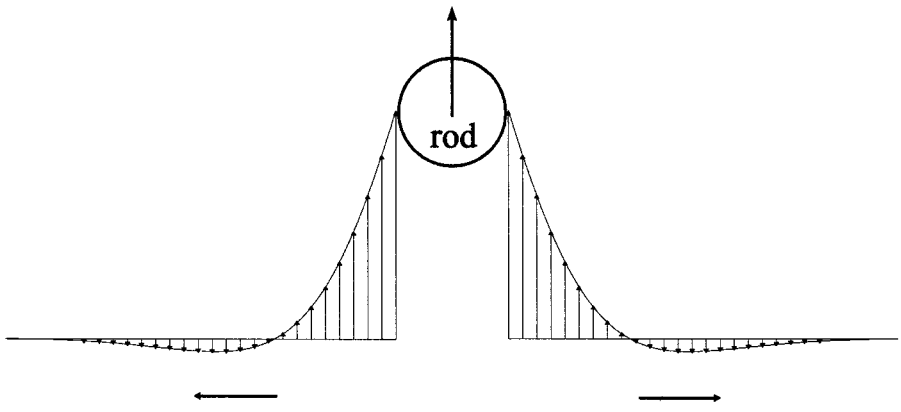

FIGURE 3 Instantaneous distribution of the particle velocities (vertical arrows) caused by a shear wave in a viscous fluid. This can be described by the mass drag effect around an oscillating rod (cross section) in a liquid. The layer nearest the rod has the highest velocity. Due to friction forces, the velocities of the following layers are diminished.

The relation between the elastic modulus E and the compression modulus K is:

$$K = \frac{E}{3 \cdot (1 - 2\mu)} \quad (12)$$

where μ is the Poisson ratio (e.g., for actin filaments about 0.4, Schmidt et al., 1996. The elastic modulus, E, is then 0.6 times the compression modulus, K).

K is often expressed as the compressibility κ: $K = 1/\kappa$.

Calculation of the amplitude of the glass fiber oscillation

The amplitude of the glass fiber oscillation is derived from the wavelength and the amplitude modulation of the ultrasound signal:

$$A = \frac{\lambda}{2} \cdot \frac{\varphi}{360^\circ} \quad (13)$$

where A is the amplitude of the glass fiber movement, λ is the wavelength of the longitudinal acoustic wave, and φ the phase shift of the ultrasound signal.

Micro falling ball viscosimeter

The sample volume of the micro falling ball viscosimeter is 300 μl. The ball ($\varnothing$ = 3.06 mm, refined steel) falls through two light barriers used for switching a digital chronometer.

The dynamic viscosity is calculated with:

$$\eta = k_{cal} \cdot (\rho_{ball} - \rho_s) \cdot t \quad (14)$$

where η is the dynamic viscosity (mPa s), ρ_{ball} is the density of the ball (g/cm^3), ρ_s is the density of the specimen (g/cm^3), t is the falling time (ms) and k_{cal} a calibration factor eliminating geometric differences of the ball and the glass tube, as given by:

$$k_{cal} = \frac{\eta_{H_2O}}{(\rho_{ball} - \rho_{H_2O}) \cdot t} \quad (15)$$

where η_{H_2O} is the standard value of water at 25°C (0.9 mPa s). The density of the ball is 7.8 g/cm^3. The accuracy of the falling ball assay is about 1%.

RESULTS

Precision of ORR measurements

Due to the nondestructiveness of ORR measurements, the final viscosities of actin gels measured with the ORR are considerably higher than those determined with the falling ball viscosimeter (Fig. 4 *A*). The polymerization rate (2–10 μM actin) was also considerably higher when determined with the ORR than when measured with a falling ball viscosimeter (Fig. 4 *B*). In both cases a sigmoidal relationship between polymerization rate and actin concentration was found, indicating the increase of self-association of actin filaments with increasing protein concentrations.

As illustrated in Fig. 4, strain must be kept as small as possible to obtain reliable viscoelastic data. The ORR allows application of strains as small as 1.6 nm and reliable viscosity data are obtained from gels of polymerizing actin (100 μM). This extreme sensitivity of the method is exemplified by increasing the amplitude of the ORR with 3-nm steps, changing the voltage at the piezoelectric actuator. In this small range of strain, the measurement obviously does not influence the result (Fig. 5). However, a sudden change of the amplitude in a range of some tens of nanometers reduces the viscosity of an actin gel, depending on the protein concentration. For example, increasing the displacement of the fiber by 34 nm (starting from 11 nm) decreases the viscosity of an f-actin gel to about 56% of the previous value (Fig. 6 *A*). Conversely, a decrease of the rod amplitude increases the viscosity. On subsequent increase/decrease cycles of the rod oscillation amplitude (Fig. 6 *A*, >300 s) in a range of 65 nm modulates the apparent viscosity; the changes decrease with time.

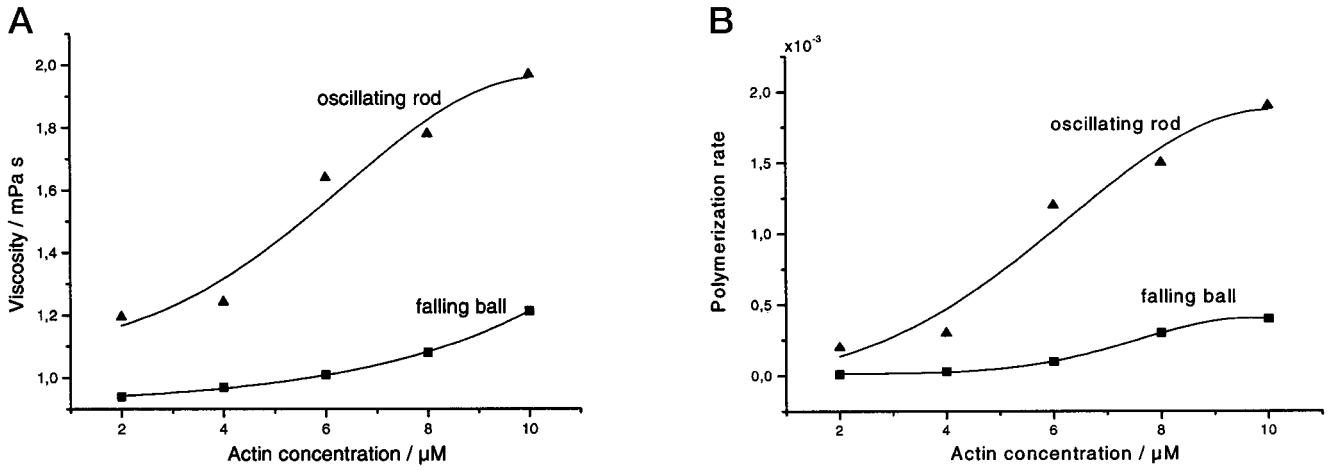

FIGURE 4 Comparison of viscosities (*A*) and polymerization rates (*B*) of a series of f-actin concentrations using a falling ball viscosimeter (■) and the ORR (▲). The differences are supposed to be the result of high (falling ball) and low (ORR) shear stress. Slopes (*B*) were calculated by fitting the almost linear viscosity increase (e.g., Fig. 8) (corresponding to the elongation phase of the actin polymerization) with the least-squares method. Symbols are representing the mean of 2–4 independent measurements. The standard deviation of six independent viscosity measurements of the same actin concentrations with the ORR was ±0.06 mPa s. Solid lines were the best fit of the data. The densities of the g-actin gels were 0.98 g/cm^3 ± 0.015 g/cm^3.

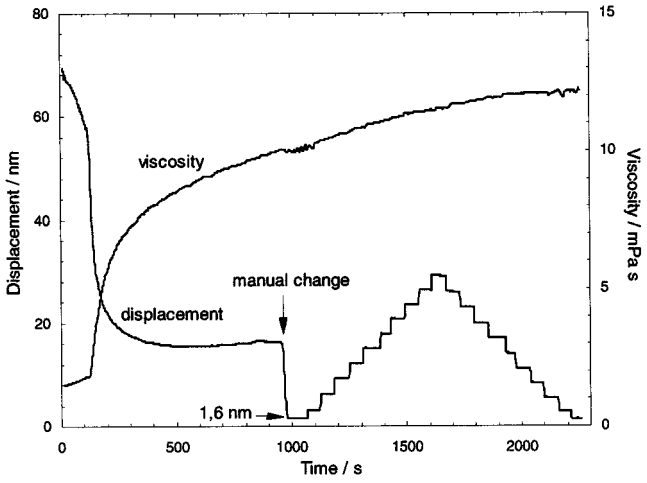

FIGURE 5 Dynamic viscosity of the sample and amplitude of the rod oscillation during polymerization of 100 μM g-actin. The amplitude of the rod oscillation was varied systematically starting at the point marked by the arrows: First the oscillation amplitude was brought to 1.6 nm and then increased/decreased in 3 nm steps. Obviously in the range up to 30 nm, these amplitudes of rod oscillation do not influence the result of the viscosity measurement.

Adding 1.6 μM α-actinin to 24 μM actin (Fig. 6 *B*), the final viscosity rises about twice that without α-actinin and, in addition, the stiffness increases due to the nucleation and bundling activity of α-actinin (Holmes et al., 1971). Subsequent decrease/increase cycles of 38 nm influenced the viscosity by only about 8% (compare actin without α-actinin: 56%, Fig. 6 *A*).

When the actin (5–100 μM) or tubulin (10–100 μM) gels were less organized, as is the case during the elongation phase, viscosity was not influenced by alterations of the rod amplitude in a range of 1–120 nm (data not shown). As a control for the instrument response function a sudden change of the amplitude of the glass rod in buffer was determined. No influence on the apparent viscosity of saline (changes $\pm$0.01 mPa s) was found.

Frequency-dependent elasticity changes upon interaction of actin with α-actinin

Elasticity of cytogels are related to strain (deformation) rate. Because the rod oscillation was adjusted by remote control to its resonance frequency (1–2.5 kHz), it was not possible to determine the dynamic viscosity and frequency dependence of elasticity synchronously.

In the range of 0.05–33 kHz of the rod oscillating frequency (amplitude, 15 nm), the elasticity (derived from sound velocity) of actin/α-actinin (molar ratio 15:1) was frequency dependent, while elasticity of actin (24 μM) without α-actinin was not (Fig. 7).

Changes in dynamic viscosity and elasticity during the polymerization of actin and tubulin

Actin polymerization was induced by adding $MgCl_2$ and KCl to the g-actin solution (10 μM). This caused an immediate rise of sound velocity (Fig. 8 *A*) due to the solid-like hydrated salt clusters (Kroebel and Mahrt, 1976) conducting acoustic waves fast. The sound velocity, and thus (volume) elasticity (Eqs. 10 and 11), during the polymerization of actin increased slightly at low actin concentrations (Fig. 8 *A*), but decreased considerably with high molar (>25 μM) actin concentrations (Fig. 8 *B*). The same effect was observed for tubulin (Fig. 9, *A* and *B*), which was induced to polymerize by heating the ice-cold solution to 37°C. The fraction of sound velocity increase due to heating of the solution to initiate tubulin polymerization has been determined by comparing sound velocity changes of tubulin-free buffer with those of tubulin (10 μM) subjected to the same heating regime (Fig. 10). The increase of the sound velocity

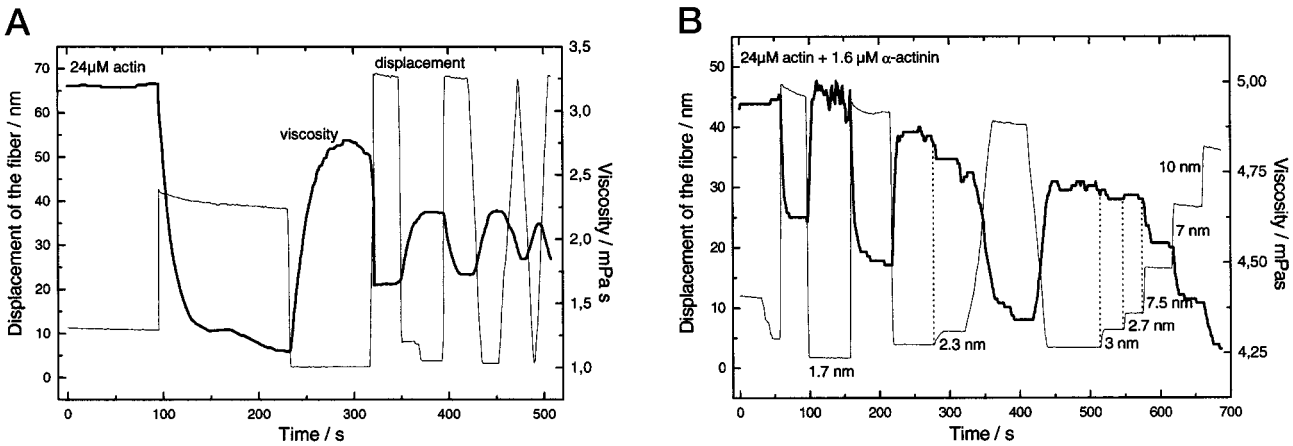

FIGURE 6 Viscosity changes of 24 μM f-actin (*A*) and 24 μM f-actin with 1.6 μM α-actinin (*B*) evoked by a sudden shift of the amplitude of the rod oscillation. An increase of the amplitude decreases the viscosity and a decrease of the amplitude increases the viscosity. α-actinin increases the final viscosity about twice that of actin without α-actinin (*B*). The change of the viscosity due to shear stress was 7 times smaller than without α-actinin. Oscillations of the viscosity values at 1.7 nm rod oscillation amplitude—after 100 s—(*B*) result from the low signal-to-noise ratio.

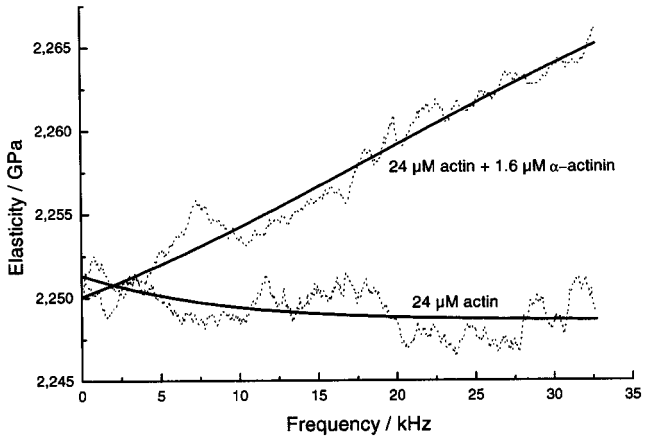

FIGURE 7 Strain rate (frequency) dependence of the elasticity of fully polymerized 24 μM f-actin and 24 μM f-actin with 1.6 μM α-actinin in buffer. The frequency of the glass fiber oscillation was increased from 50 Hz to 33 kHz. The solid curves represent the fit of curves by the least squares method. Though the curves are the mean of 2 (actin) to 4 (actin/α-actinin) independent measurements, elasticity varied, presumably due to a thermostatic inaccuracy. However, it is obvious that the elasticity of actin/α-actinin was frequency-dependent, whereas that of pure f-actin was not.

of the tubulin gel prior to viscosity changes was 20 times higher than that of the pure buffer.

During the polymerization of actin the sound velocity increased up to +1.3 m/s (corresponding to an elastic modulus of 1.69 kPa) in low concentration solutions (2 μM) and decreased up to −7 m/s (≅49 kPa) at high concentrations (100 μM). On polymerization of tubulin a concentration-dependent decrease of sound velocity was also observed (+48 to −12 m/s ≅ 2.3–0.1 MPa, for 10- to 100-μM tubulin).

For f-actin gels (2–100 μM) a final viscosity of 1.3–9.4 mPa s and a final elastic modulus (calculated from the sound velocity) of 2.229–2.254 GPa have been determined (Fig. 11 *A*). For microtubule gels (10–100 μM) a final viscosity of 1.5–124 mPa s and a final elastic modulus of 2.288–2.547 GPa have been determined (Fig. 11 *B*). For both the polymerized proteins actin as well as tubulin, the decrease of elasticity approaches a minimum value. Thus, exceeding a specific protein concentration does not alter the filament aggregation status further.

As discussed below, the decrease is suggested to be due to the packing density, followed by a nematic phase transition from a liquid to a liquid-crystal phase where packing density reached its maximum. This phase transition occurs in the range of 8–50 μM for f-actin and of 25–85 μM for microtubules. No rheological differences of various concentrations of g-actin (see Fig. 8, *A* and *B*, before salt is added) and tubulin (see Fig. 9, *A* and *B*, at the beginning of the measurement) were found. Therefore, the packing effect is not a protein concentration effect.

Modulation of viscoelasticity by ATP

ATP (2 mM) increased actin polymerization when compared with 0.2 mM ATP (Fig. 12 *A*). Simultaneously, the increase of sound velocity revealed higher elasticity due to ATP (Fig. 12 *B*). This effect was in the presence of glucose totally abolished when ATP was depleted by the glycolytic enzyme hexokinase (Fig. 12 *B*), although this actin binding enzyme (type I from bovine heart) in the absence of glucose accelerates the polymerization rate and increases the final viscosity of actin (Fig. 12 *A*). In electron micrographs actin filaments with hexokinase (same conditions as in Fig. 12) appeared shorter than without hexokinase (Fig. 13, *A* and *B*).

Viscoelastic changes during the interaction of actin with phalloidin

Fig. 14 *A* shows the typical exponential viscosity time course of actin polymerization in the presence of phalloidin

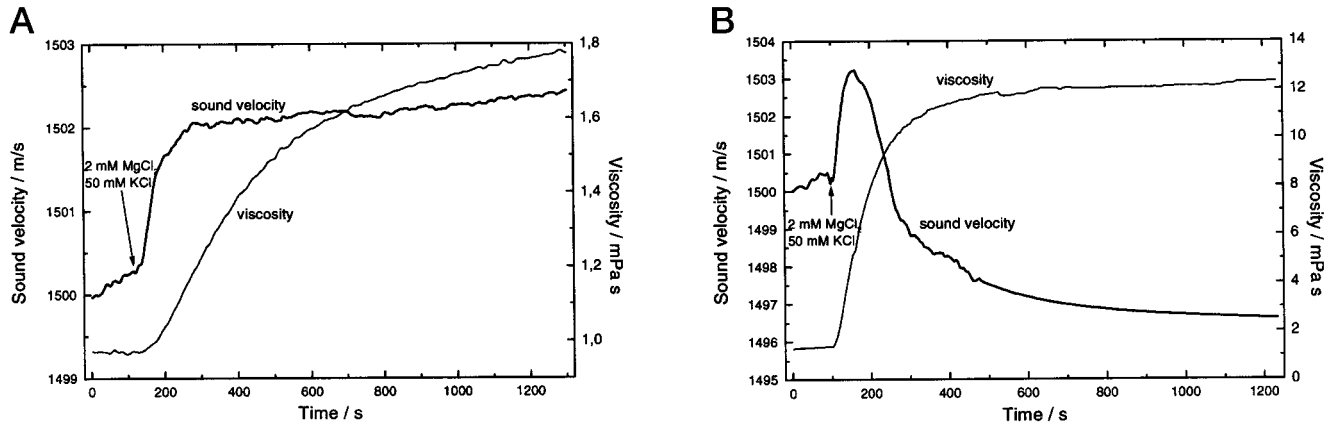

FIGURE 8 Dynamic viscosity and sound velocity changes during the polymerization of (*A*) 10 μM and (*B*) 100 μM actin. The increase of the sound velocity (about 0.5 m/s) at the very beginning is due to the heating of the cold suspension. The subsequent increase of 2–2.5 m/s of the sound velocity is due to the added salt. A small increase of sound velocity (0.4 m/s) during the polymerization of 10 μM (*A*) actin and a larger decrease of the sound velocity (6.5 m/s) of 100 μM actin (*B*) indicate concentration-dependent elasticity changes of the actin network.

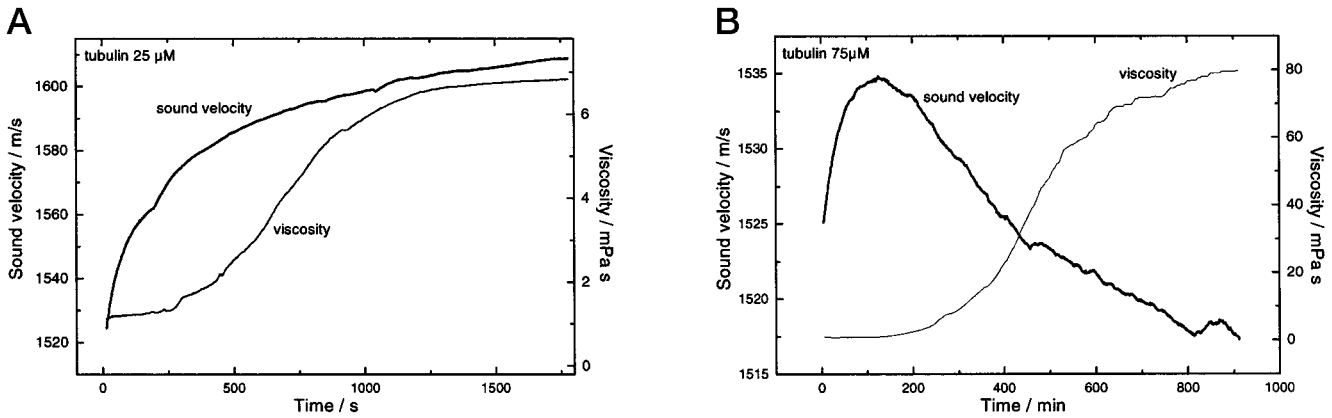

FIGURE 9 Upon tubulin (25 μM) polymerization evoked by a rise in temperature, sound velocity increases up to 60 m/s before any change of the viscosity. During the elongation phase, represented by the viscosity increase, sound velocity increases more slowly. *A*: 25 μM tubulin. *B*: 75 μM tubulin.

as was described by Dancker et al. (1975). The final viscosity is higher than without phalloidin (compare Figs. 8 *A* and 14 *A*), because of enhanced polymerization, due to the reduced critical g-actin concentration (Estes et al., 1981). While sound velocity increases slightly during the polymerization of 10 μM of g-actin without phalloidin (Fig. 8 *A*), it decreases by about 2 m/s in the presence of phalloidin. This means that sound velocity of actin (10–11 μM) associated with phalloidin is about 4.5 m/s ($\cong$20.3 kPa) lower than without phalloidin.

DISCUSSION

Comparison of the ORR with other types of rheometer

The main advantage of the ORR is the possibility for synchronous measurements of dynamic viscosity and sound velocity (equivalent to elasticity), as well as the extremely small strain and the ratio of the dimension of the sensor to the penetration depth of the viscosity shear wave. Since the amplitude of the moving glass rod is in the nanometer range and freely variable, interactions and properties of macromolecules can be determined nondestructively (Fig. 5).

Measurements of viscoelastic properties of actin gels using minimum strain were also achieved by Zaner et al. (1981) and Sato et al. (1985) with cone-plate rheometers. However, the sample volume was some milliliters and (as for most rheometers) during the measurement, the device has to be closed. Because the ORR requires only a few microliters and it is an open system, the online addition of substances allows a broad range of experimental control.

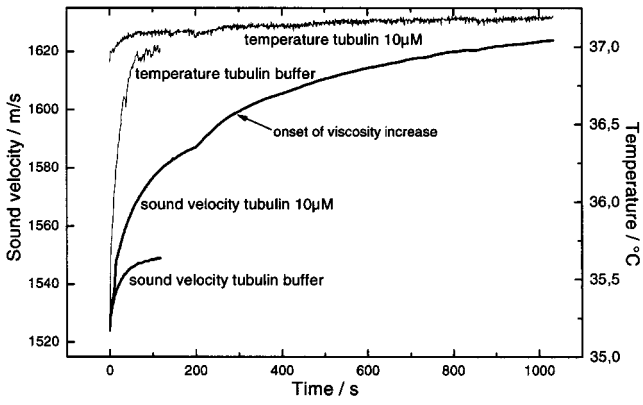

FIGURE 10 Temperature of tubulin buffer and tubulin solution rise very fast with heating. The heating of the tubulin buffer corresponding to induction of polymerization, accelerated sound velocity by 3 m/s what is much less than the sound velocity increase of 60 m/s accompanying polymerization.

Precision of the ORR

The final viscosities and polymerization rates of actin gels, determined with the falling ball viscosimeter and the ORR, differed considerably (Fig. 4, *A* and *B*). The differences are supposed to result from differences in strain imposed by the measuring device. The almost sigmoidal relationship between the final f-actin viscosities and actin concentrations (Fig. 4 *A*), could result from bundling with increasing protein concentration (Griffith and Pollard, 1982; Tang and Janmey, 1996).

Polymerization rate, was considerably higher when measured using the ORR (Fig. 4 *B*). This observation contradicts the widespread opinion that shear stress enhances the rate of polymerization due to an increased availability of nucleating oligomers derived from broken filaments (Cooper and Pollard, 1982). The sigmoidal increase (now more obvious for the falling ball assay, too) points to an enhanced self-association of actin filaments with increasing protein concentration.

Because the ORR is not air-sealed, evaporation may influence measurements. Because of the overall construction, evaporation from the specimen drop is very small. This is demonstrated by a change of less than 0.01 mPa s for the viscosity of actin buffer measured for 40 min.

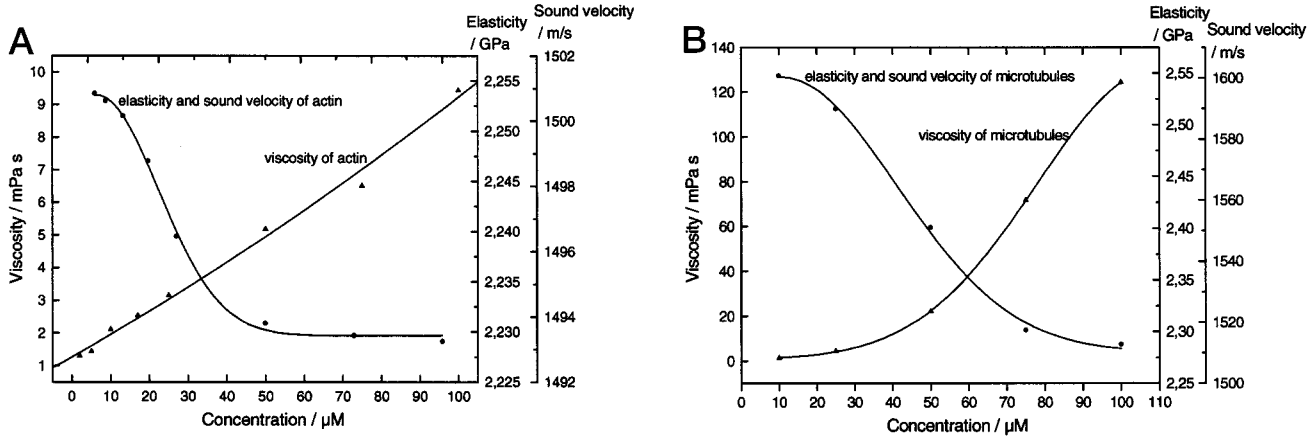

FIGURE 11 Viscoelasticity of f-actin (*A*) and microtubule (*B*) gels, determined with the ORR. Viscosity = ●; elasticity and sound velocity = ▲. Sound velocities of f-actin (monitored at 25°C) and microtubule gels (monitored at 37°C) of different concentrations were determined at the beginning of the polymerization steady-state phase. The change of the sound velocity of f-actin gels was +10 to −10 m/s (corresponding to 0.1 MPa) for 5–100 μM actin gels. The sound velocity change of 2.5 m/s, caused by the salt, was subtracted for each actin concentration. For 10–100 μM of microtubule gels the change was +50 to −10 m/s (corresponding to 2.5 MPa and 0.1 MPa) (corrected for temperature dependence of sound velocity of the buffer). One symbol represents the mean of 2 to 5 different measurements.

Viscoelastic properties of actin and actin/α-actinin gels

During actin polymerization, the amplitude of the glass fiber oscillation, which is in the range of 1–50 nm depending on sensor dimensions and viscosity, decreases; therefore, strain rate is also diminished. Strain and strain rate in the ORR do not influence viscosity measurements (Fig. 5). Therefore the values are considered to represent true viscosity.

The apparent viscosity of actin gels drops after a sudden increase of strain exposure (Fig. 6 *A*). The change of the viscosity with varying amplitude of the rod oscillation reflects the typical non-Newtonian behavior of f-actin: high shear stress (Fig. 4 *A*) results in low apparent viscosities (breaking and deformation of filaments). Such an abrupt decrease of viscoelasticity was also observed by Janmey et al. (1990) when strain amplitudes exceeded 20% (determined with cone-plate rheometer at 1 rad/s with maximal strain of 50% which was 1.4 Pa). The fast viscosity recovery after disruption (Fig. 6 *A*) presumably is due to annealing of actin filaments.

Periodic application of high strain increasingly destroys the actin network. Initially, the entangled networks may repair themselves, but this recovery process diminishes, and the networks became irreversibly altered around the rod (Fig. 6 *A*, >300 s). Nucleation of actin is enhanced by α-actinin, thus rendering the resistance to strain and reannealing more efficient (Fig. 6 *B*).

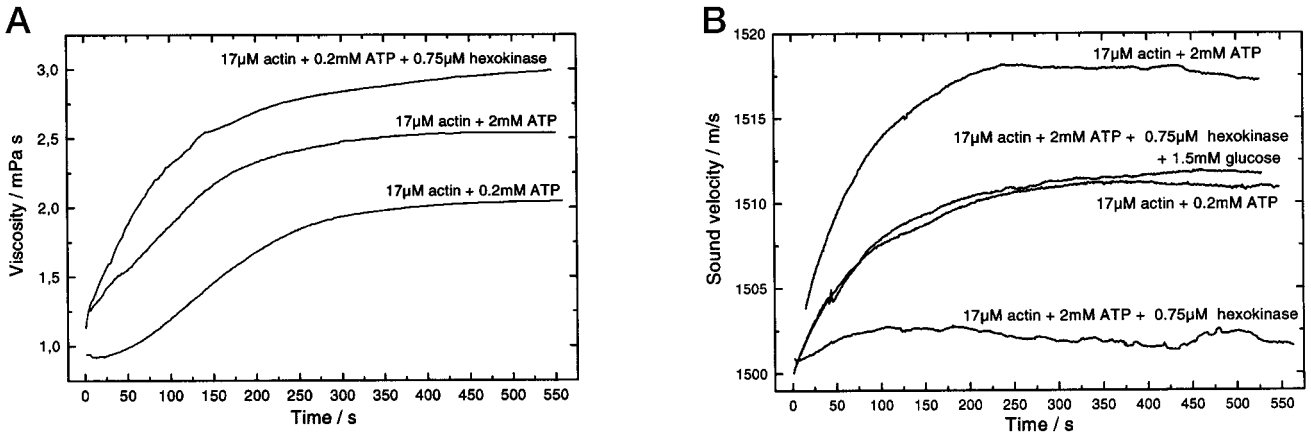

FIGURE 12 *A*: Polymerization kinetics of 17 μM actin as revealed by viscosity changes. ATP (2 mM) and hexokinase (0.75 μM) increase polymerization rate and final viscosity as well. *B*: Elasticity of f-actin during polymerization as revealed by increasing sound velocity. ATP (2 mM) stiffens the actin fibrils, in presence of hexokinase (without glucose) this stiffening is abolished and fibril elasticity is very much reduced. In the presence of its substrate glucose, hexokinase does not influence f-actin stiffness, that corresponds to the value determined by the ATP-concentration. Curves are the mean of 3–7 independent measurements.

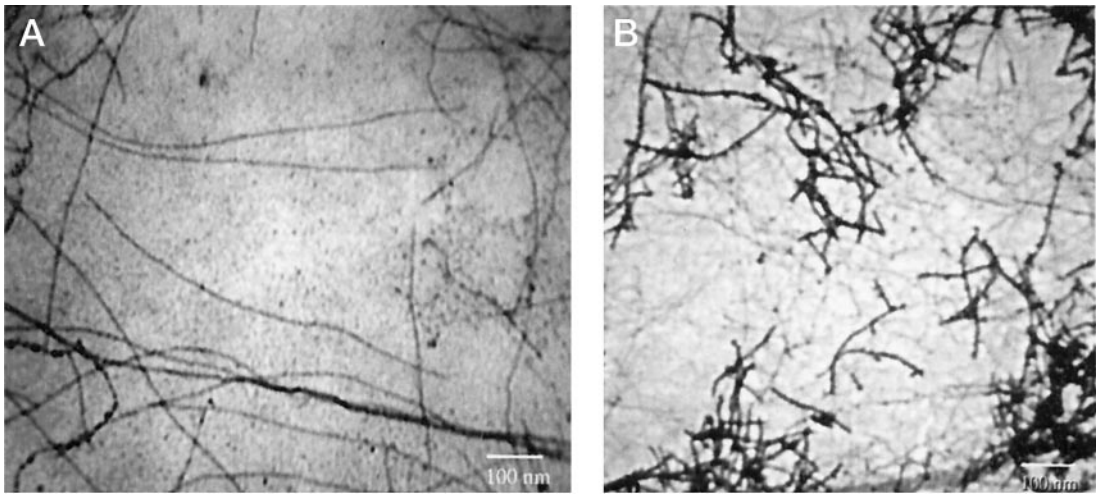

FIGURE 13 *A*: EM pictures of negative-stained f-actin filaments (17 μM) after 10 min polymerization. *B*: Same condition as (*A*) with 0.75 μM hexokinase added to g-actin before inducing the polymerization with a final concentration of 50 mM KCl and 2 mM $MgCl_2$. Short actin fibrils appeared.

Strain applied with the ORR contains two components: the strain caused by the ultrasound signal (1 GHz) and the strain caused by the glass fiber oscillations (1–3 kHz). Due to the extremely high frequency of the ultrasound signal this component can be regarded as truly nondestructive and only the elastic properties of the specimen are revealed. Low frequency strain (3 kHz), caused by the glass rod also is nondestructive for small amplitudes and did not change elasticity of actin in the frequency range of 50 Hz to 33 kHz (Fig. 7), fulfilling the criteria defined for long rods by Zaner and Stossel (1983): long filaments impede each others' rotational diffusion and thus, no additional energy is stored. However, actin/α-actinin gels (12:1 molar ratio) revealed a frequency (50 Hz to 33 kHz)-dependent increase of elasticity (Fig. 7). The elasticity values determined represent the mean over the distance from the lens to the surface of the oscillating rod and do not take into account any inhomogeneities of elasticity between the immediate surroundings of the rod and zones further apart.

The frequency dependence of the elasticity of actin strongly depends on filament length: in samples with long filaments storage modulus G′ and loss modulus G″ are frequency-independent over the range of 0.01–100 rad/s. In comparison, in actin samples with short filaments (derived by adding gelsolin) G′ and G″ become frequency-dependent (Janmey et al., 1990). The viscoelasticity (G′ and η) of actin/α-actinin (12:1 molar ratio), is increased when compared to pure actin, and in addition increases 40-fold when deformed (strained) at 1 Hz (Sato et al., 1987). The frequency dependence of actin/α-actinin (Fig. 7) and the viscous resistance (Fig. 6 *B*) correspond to properties of short and flexible rods (Zaner and Stossel, 1983). Xu et al. (1998) provide evidence that α-actinin forms dynamic cross-links between actin filaments (as described by Sato et al., 1987)

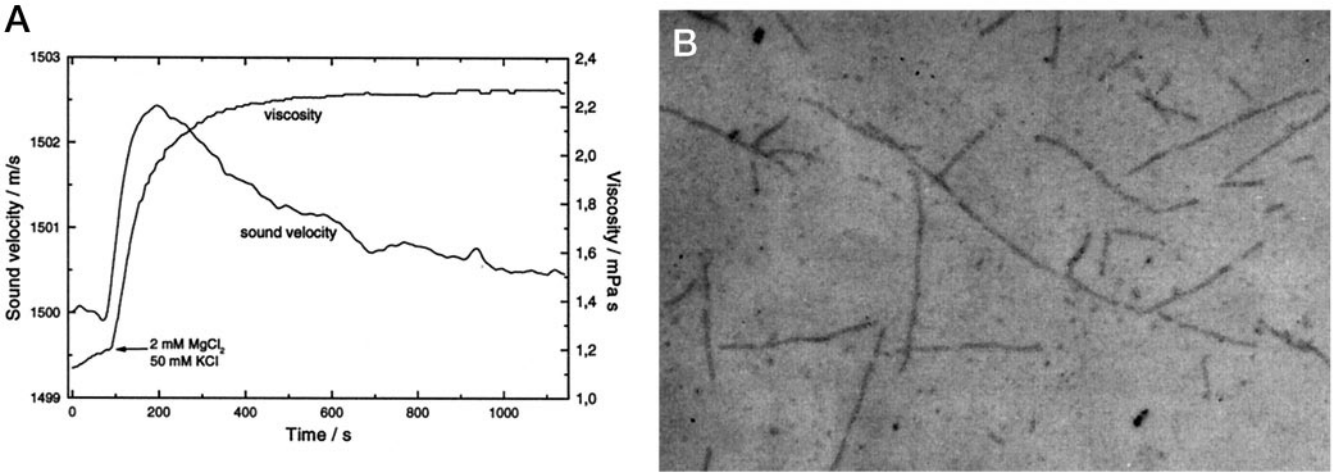

FIGURE 14 Time course of viscosity and sound velocity changes during the polymerization of 10 μM actin with 5 μM phalloidin (*A*). After an initial phase of sound velocity increase (corresponding to that found without phalloidin) (Fig. 8 *A*), a phase of sound velocity decrease (2 m/s) followed. The kinky appearance of actin filaments in the electron micrograph correspond well to the decreased stiffness calculated from the sound velocity measurements (*B*).

that might explain the duality of actin/α-actinin networks: at low rates of deformation the network has the same stiffness as f-actin alone, but it responds with high resistance at high rates of deformation.

α-actinin enhances the polymerization rate of actin, because it acts as a nucleating protein (Pollard and Cooper, 1986). By cross-linking, it increases the viscosity up to twofold (Fig. 6) (Holmes et al., 1971). α-actinin bundles actin filaments at high ratios of α-actinin to actin (then the entangled network behaves as a viscous fluid), whereas at low ratios an isotropic network is formed with the mechanical properties of an elastic solid (Dancker et al., 1975). The viscous fluid character of a gel containing a high molar ratio of actin/α-actinin (2:1) was also confirmed by its low sound velocity, which did not differ from that of pure actin (data not shown).

Concentration-dependent viscoelasticity of f-actin

A protein-fibril gel can be described as a two-phase system, the solvent (saline) with a high compression modulus and the solid (protein) with a lower, unknown compression modulus. With increasing protein concentration its volume fraction increases and thus, the contribution of this phase (with the lower compression modulus) increases, i.e., the overall compressibility (corresponding to the volume elasticity) decreases (Fig. 15). In addition, protein filaments bind less solvent molecules than the monomers, which decreases the compression modulus component introduced by hydration shells.

The commonly used frequency dependent shear modulus G′ (dynamic storage modulus, indicating stored mechanical energy, e.g., resistance to deformation by shear forces) and G″ (dynamic loss modulus, indicating dissipated mechanical energy, that is, viscous resistance) cannot be directly compared with the elastic modulus, derived from the sound velocity at 1 GHz (Eq. 12). Unfortunately measurements of G′ of actin gels reported in the literature differ largely: during polymerization of 50 μM actin, values of about 10–1000 Pa have been determined with different rheometers in different laboratories (Janmey et al., 1994).

Sound velocity measurements of polymerized actin were performed by Suzuki et al. (1996) with what they called a sing-around pulse method. They observed a decrease of the compressibility during actin polymerization. For 50–150 μM of actin the sound velocity differed by 1.5 m/s. The authors explained this small concentration-related difference by interactions of f-actin filaments. According to the present study, the sound velocity of polymerized actin is almost independent of protein concentrations in the range used by Suzuki et al. (1996) (Fig. 11). The authors also determined a positive partial specific adiabatic compressibility of g-actin of $9.3 \cdot 10^{-12}$ Pa^{-1} and a negative compressibility of f-actin of $-12.7 \cdot 10^{-12}$ Pa^{-1}. The partial specific adiabatic compressibility β_s (Pa^{-1}) was calculated as followed:

$$\beta_s = \frac{\beta_0}{\upsilon_0}\left(-\frac{2 \cdot 10^3}{u_0} + \left(\frac{\Delta u}{c}\right)_{\lim c \to o} - \frac{1}{\rho_0} + 2\upsilon_0\right) \quad (16)$$

where $\beta_0 = 1/(\rho_0 u_0^2)$ is the adiabatic compressibility of the solvent (Pa^{-1}), ν_0 is the partial specific volume of actin in solution (cm^3/g) (calculated via density determinations), u_0 is the sound velocity of the solvent (cm/s), $\Delta u = u - u_0$ (where u is the sound velocity of the protein solution) and ρ_0 is the density of the solvent (g/ml).

Using Eq. 16, we calculated the partial specific adiabatic compressibility, with $\nu_0 = 0.632$ cm^3/g as determined by Suzuki et al. (1996), $\rho_0 = 0.998$, $u_0 = 149800$ cm/s (25°C) and $(\Delta u/c)_{\lim c \to o} = -10$ cm/s (derived from the f-actin measurements as shown in Fig. 11 *A*) and obtained a value of $-6.9 \cdot 10^{-10}$ Pa^{-1}, which is also negative but two orders of magnitude higher than $-12.7 \cdot 10^{-12}$ Pa^{-1}, determined by Suzuki et al. (1996). This difference is related to differences in actin concentrations: as mentioned before, Suzuki et al. (1996) examined only high molar actin concentrations (50–145 μM) to determine $(\Delta u/c)_{\lim c \to o}$. In the present study low and high actin concentrations (2–100 μM) have been examined (Fig. 11 *A*).

The differences in the frequency of the used ultrasound signal should also be mentioned. Suzuki et al. (1996) used 5 MHz to determine the sound velocity, whereas the ORR operated with 1 GHz. However, compressibility of actin (in contrast to attenuation) can be considered independent of the frequency of ultrasound waves in the range between 1 MHz and 1 GHz; molecular relaxation time influences can be expected to appear in the range above 10 GHz.

Concentration-dependent viscoelasticity of microtubule gels

Brown and Berlin (1985) analyzed the specific volume of microtubules by centrifugation. The standardized packing volume of microtubules without MAPs was 10.3 ± 2.3 μl/mg protein (corresponding to 120 μM tubulin). If the decrease of the sound velocity with increasing microtubule concentration reflects increasing packing density (Fig. 11 *B*), then, extrapolating the elasticity curve in Fig. 11 *B* to its expected saturation value would yield 120 μM. The highest packing density of actin as calculated from the values shown in Fig. 11 *B* is reached at 60 μM, almost half that of the microtubule concentration, although the actin filament is about 4 times thinner than a microtubule. The charge density and therefore the amount of hydration of the actin filament and the microtubule differ considerably.

Measurements of viscoelastic properties of microtubules are rare. Olmsted and Borisy (1973), using an Ostwald capillary viscosimeter, obtained a sigmoidal course of the viscosity/concentration curve (10–110 μM) similar to that in Fig. 11 *B*, indicating length variation of microtubules or low affinity interactions between microtubules with rising concentrations. A falling ball assay was performed by

Brown and Berlin (1985) for 45 μM of tubulin. The dynamic viscosity varied between 75 and 175 cP (=mPa s) at pH 6.7. We determined 20 mPa s for a 45-μM solution. However, these authors used taxol-stabilized microtubules, so higher viscosity values should be expected (Howard and Timasheff, 1988).

A variety of polymorphic tubulin assembly products in vitro (visualized with electron microscopy) were described in detail by Unger et al. (1990), e.g., rings, spirals, ring-crystals, ring fragments, 10-nm fibers, hoops, and sheets (also visualized with SFM by Vater et al., 1995). The assembly of dimers forming these solid-like structures before the elongation process could be responsible for the high increase of the sound velocity early during polymerization (Fig. 9). Therefore, it is not surprising that low concentrations of microtubules are indistinguishable on the basis of viscosity measurements from unpolymerized tubulin as described by Sato et al. (1988). The strongest change of elasticity was found between 25 and 85 μM (Fig. 11 *B*). In this range a nematic phase transition between randomly oriented (flexible) rods (Sato et al., 1988) and liquid crystal formation (Buxbaum et al., 1987) occurs. Above 85 μM, liquid crystal formation may be approximated by highest packing density. However, comparison of the viscoelastic properties of fibrin (forming isotropic networks without lateral aggregation) with actin gels revealed that liquid crystal formation is not necessary for polymer solutions to be viscoelastic (Janmey et al., 1991).

Fig. 15 visualizes a model to explain the concentration dependence of compressibility. At high protein concentrations competition of the protein molecules for water reduces the hydration shell per molecule, a phenomenon that also accompanies g-to-f transition and results in a decrease of the compression modulus. This hypothesis is also in accord with measurements of Suzuki et al. (1996), which revealed a reduction of hydration water of 1 ml/g protein on polymerization of actin. Considering the large influence of water on the elasticity of polymer gels, the frequency used for rheometry contributes to differences between E and G′ of some orders of magnitude: e.g., Janmey et al. (1991) determined with a torsion pendulum at 1 rad/s values of G′ of 283 Pa for f-actin (50 μM) and 34 Pa for microtubule gels (50 μM); with the ORR at 1 GHz, changes in E values of 25 kPa during the polymerization of actin (50 μM) and 400 kPa for microtubule gels (50 μM) have been determined.

ATP-induced viscoelastic changes of actin

ATP and pyrophosphate stabilize actin fibrils (Dancker and Fischer, 1989). The influence of ATP on actin filament stiffness was first studied by Janmey et al. (1990). They compared the properties of polymerized ATP-actin and ADP-actin (prepared by the addition of 1 mM glucose and yeast hexokinase to monomeric ATP-actin, as described by Pollard, 1984): ADP-actin filaments seemed to be more flexible and, conversely, ATP-actin filaments stiffer. These results were disputed by Pollard et al. (1992) and Newman et al. (1993), who did not detect remarkable rheological differences. The small rheological differences between ATP-actin and ADP-actin were explained by alterations of the filament length. With the ORR an increase of final viscosity and the overall elasticity of actin gels was found when increasing the ATP concentration from 0.2 to 2 mM in the polymerization buffer. This effect was easily reversible by adding hexokinase plus glucose (Fig. 12 *B*) to reduce the ATP concentration.

Hexokinase in the absence of glucose has properties similar to capping proteins as gelsolin, fragmin, villin, or scinderin (Hartwig and Kwiatkowski, 1991; Pollard and Cooper, 1986): it reduces the lag phase and increases final viscosity and the polymerization rate (Fig. 12 *A*). In addition, elasticity decreases (Fig. 12 *B*) by shortening of the filaments (Fig. 13 *B*). This similarity to the behavior of other capping and nucleating proteins explains neither the mechanism of nucleation nor the mechanism of severing. Pollard (1984), using *Acanthamoeba* actin and yeast hexokinase, did not find any influence of hexokinase on actin polymerization. This could be due to different binding properties of the respective proteins.

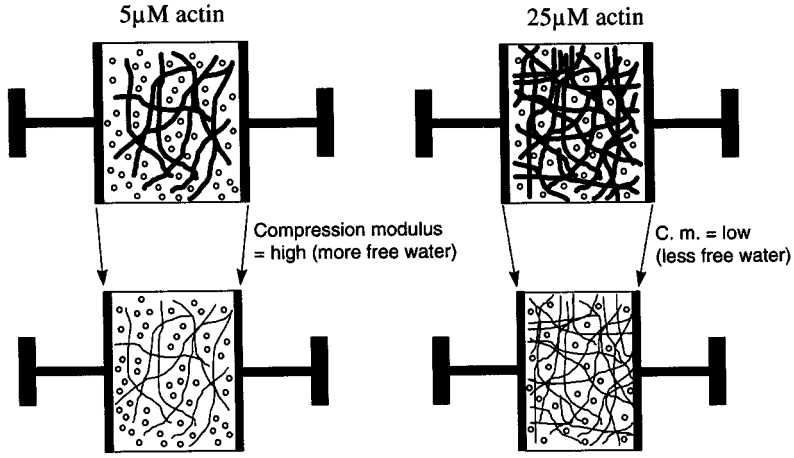

FIGURE 15 Model illustrating the change of the elastic modulus during the polymerization of low and high g-actin concentrations in solution.

Viscoelastic changes of actin upon interaction with phalloidin

Phalloidin, a heptapeptide toxin from the mushroom *Amanita phalloides*, stabilizes actin filaments by preventing monomer dissociation from both ends. It decreases the association rate constant of actin at the barbed end by about 50% and retards the release of P_i from ATP-hydrolysis (Dancker and Hess, 1990; De La Cruz and Pollard, 1994). Phalloidin enhances the polymerization rate (Dancker et al., 1975) and increases the extent of polymerization because of reduction of critical actin concentration (Estes et al., 1981).

The exponential viscosity time course upon polymerization of actin in the presence of phalloidin (Fig. 14 *A*) was expected and had previously been described (Dancker et al., 1975). The simultaneous decrease of the sound velocity was unusual for an actin concentration of 10 μM and revealed that phalloidin f-actin is more flexible than unconjugated actin, a result confirmed by the kinked appearance of the electron micrograph (Fig. 14 *B*).

We thank Dipl.-Phys. K. Hillmann, Dr. Z. Kojro, and Dipl.-Phys. E. von der Burg. They have contributed enormously to the practical and theoretical development of the ORR. We also thank Dr. T. Müller-Reichert from the EMBL in Heidelberg for preparing the tubulin, Mr. P. Walzer, who turned the very small components of the construction with high precision, and E. Weichselsdorfer for the electron micrographs in Fig. 14 *B*.

Support by the DFG is gratefully acknowledged (grants Be 423/13, 15, and 16).

REFERENCES

Ashford, J. A., S. S. L. Andersen, and A. A. Hyman. 1998. Preparation of tubulin from bovine brain. *Cell Biology: A Laboratory Handbook.* 2nd Ed., Vol. 2. Academic Press, San Diego. 205–212.

Bereiter-Hahn, J. 1994. Mechanical basis of cell shape and differentiation. Mechanische Grundlagen von Zellform und Zelldifferentierung. *Verh. Dtsch. Zool. Ges.* 872:129–145.

Bereiter-Hahn, J. 1995. Probing biological cells and tissues with acoustic microscopy. *In* Advances in Acoustic Microscopy. A. Briggs, ed. Plenum Press, New York. 79–115.

Bereiter-Hahn, J., I. Karl, H. Lüers, and M. Vöth. 1995. Mechanical basis of cell shape: investigations with the scanning acoustic microscope. *Biochem. Cell. Biol.* 73:337–348.

Bereiter-Hahn, J. 1997. Supramolecular associations with the cytomatrix and their relevance in metabolic control: Protein synthesis and glycolysis. *Zoology.* 100:1–24.

Bereiter-Hahn, J., and H. Lüers. 1998. Subcellular tension fields and mechanical resistance of the lamella front related to the direction of locomotion. *Cell Biochem. Biophys.* 29:14–17.

Bradford, M. 1976. A rapid and sensitive method for the quantities of protein utilizing the principle of protein-dye binding. *Anal. Biochem.* 72:248–254.

Brown, P. A., and R. D. Berlin. 1985. Packing volume of sedimented microtubules: regulation and potential relationship to an intracellular matrix. *J. Cell Biol.* 101:1492–1500.

Buxbaum, R. E., T. Dennerll, S. Weiss, and S. T. Heidemann. 1987. F-actin and microtubule suspensions as indeterminate fluids. *Science.* 235: 1511–1514.

Cooper, J. A., and T. D. Pollard. 1982. Methods to measure actin polymerization. *Meth. Enzymol.* 85:182–210.

Dancker, P., I. Löw, W. Hasselbach, and T. Wieland. 1975. *Biochim. Biophys. Acta.* 400:407–414.

Dancker, P., and S. Fischer. 1989. Stabilization of actin filaments by ATP and inorganic phosphate. *Z. Naturforsch. C.* 44:698–704.

Dancker, P., and L. Hess. 1990. Phalloidin reduces the release of inorganic phosphate during actin polymerization. *Biochim. Biophys. Acta.* 1035: 197–200.

De La Cruz, E. M., and T. D. Pollard. 1994. Transient kinetic analysis of rhodamine phalloidin binding to actin filaments. *Biochemistry.* 33: 14387–14392.

Emerman, J. T., and D. R. Pitelka. 1977. Maintenance and induction of morphological differentiation in dissociated mammary epithelium on floating collagen membranes. *In Vitro.* 13:316–328.

Estes, J. E., L. A. Selden, and L. C. Gershman. 1981. Mechanism of action of phalloidin on the polymerization of actin. *Biochemistry.* 20:708–712.

Feramisco, J. R., and K. J. Burridge. 1980. A rapid purification of α-actinin, filamin, and a 130,000-dalton protein from smooth muscle. *J. Biol. Chem.* 255:1194–1199.

Griffith, L. M., and T. D. Pollard. 1982. Cross-linking of actin filament networks by self-association and actin-binding macromolecules. *J. Biol. Chem.* 257:9135–9142.

Grill, W., K. Hillmann, K. U. Würz, and J. Wesner. 1996. Scanning ultrasonic microscopy with phase contrast. *Adv. Acoustic Microsc.* 2:167–218.

Hartwig, J. H., and D. J. Kwiatkowski. 1991. Actin-binding proteins. *Curr. Opin. Cell Biol.* 3:87–97.

Hillmann, K., W. Grill, and J. Bereiter-Hahn. 1994. Determination of ultrasonic attenuation in small samples of solid material by scanning acoustic microscopy with phase contrast. *J. Alloys Compounds* 211/212: 625–627.

Holmes, G. R., D. E. Goll, and A. Suzuki. 1971. Effect of α-actinin on actin viscosity. *Biochim. Biophys. Acta.* 253:240–253.

Howard, W. D., and S. N. Timasheff. 1988. Linkages between the effects of taxol, colchicine, and GTP on tubulin polymerization. *J. Biol. Chem.* 263:1342–1364.

Ingber, D. E. 1993. Cellular tensegrity: defining new rules of biological design that govern the cytoskeleton. *J. Cell Sci.* 104:613–627.

Janmey, P. A., S. Hvidt, J. Lamb, and T. P. Stossel. 1990. Resemblance of actin-binding protein/actin gels to covalently crosslinked networks. *Nature.* 345:89–92.

Janmey, P. A., S. Hvidt, G. F. Oster, J. Lamb, T. D. Stossel, and J. H. Hartwig. 1990. Effect of ATP on actin stiffness. *Nature.* 347:95–99.

Janmey, P. A., U. Euteneuer, P. Traub, and M. Schliwa. 1991. Viscoelastic properties of vimentin compared with other filamentous biopolymer networks. *J. Cell Biol.* 113:155–160.

Janmey, P. A., S. Hvidt, J. Käs, D. Lerche, A. Maggs, E. Sackmann, M. Schliwa, and T. P. Stossel. 1994. The mechanical properties of actin gels. *J. Biol. Chem.* 269:32503–32513.

Kojro, Z., E. v. d. Burg, J. Zinke, K. Hillmann, and W. Grill. 1996. Viscosity shear waves and mass drag effect in liquids. *Z. Phys. B.* 101:433–439.

Kroebel, W., and K.-H. Mahrt. 1976. Sound velocity in pure and sea water. *Acoustica.* 35.

Lamb, H. 1932. Hydrodynamics, 6th ed. Dover Publications, New York.

Landau, L. D., and E. M. Lifshitz. 1987. Course of Theoretical Physics. 2nd ed., vol. 6. Fluid Mechanics. Pergamon Press, Oxford.

Leung, W. P., K. C. Cho, Y. M. Lo, and C. L. Choy. 1986. Adiabatic compressibility of myoglobin. Effect of axial ligand and denaturation. *Biochim. Biophys. Acta.* 870:148–153.

Lüers, H., J. Bereiter-Hahn, and J. Litniewski. 1992. SAM Investigations: the structural basis of cell surface stiffness of cultured cells. 1992. *Acoustical Imaging.* 19:511–516.

Newman, J., K. S. Zaner, K. L. Schick, L. C. Gershman, L. A. Selden, H. J. Kinosian, J. L. Travis, and J. E. Estes. 1993. Nucleotide exchange and rheometric studies with F-actin prepared from ATP- or ADP-monomeric actin. *Biophys. J.* 64:1559–1566.

Olmsted, J. B., and G. G. Borisy. 1973. Characterization of microtubule assembly in porcine brain extracts by viscometry. *Biochemistry.* 12: 4282–4289.

Pollard, T. D. 1984. Polymerization of ADP-actin. *J. Cell Biol.* 99: 769–777.

Pollard, T. D., and J. A. Cooper. 1986. Actin and actin binding proteins: a critical evaluation of mechanism and function. *Annu. Rev. Biochem.* 55:987–1035.

Pollard, T. D., I. Goldberg, and W. H. Schwarz. 1992. Nucleotide exchange, structure, and mechanical properties of filaments assembled from ATP-actin and ADP-actin. *J. Biol. Chem.* 267:20339–20345.

Sato, M., G. Leimbach, W. H. Schwarz, and T. D. Pollard. 1985. Mechanical properties of actin. *J. Biol. Chem.* 260:8585–8592.

Sato, M., W. H. Schwarz, and T. D. Pollard. 1987. Dependence of the mechanical properties of actin/α-actinin gels on deformation rate. *Nature.* 325:829–830.

Sato, M., W. S. Schwartz, S. C. Selden, and T. D. Pollard. 1988. Mechanical properties of brain tubulin and microtubules. *J. Cell Biol.* 106: 1205–1211.

Schmidt, F. G., F. Ziemann, and E. Sackmann. 1996. Shear field mapping in actin networks by using magnetic tweezers. *Eur. Biophys. J.* 24: 348–353.

Spudich, J. A., and S. Watt. 1971. The regulation of rabbit skeletal muscle contraction. *J. Biol. Chem.* 246:4866–4871.

Suzuki, N., Y. Tamura, and K. Mihashi. 1996. Compressibility of specific volume of actin decrease upon G to F transformation. *Biochim. Biophys. Acta.* 1292:265–272.

Tamura, Y., N. Suzuki, and K. Mihashi. 1993. Adiabatic compressibility of myosin subfragment-1 and heavy meromyosin with or without nucleotide. *Biophys. J.* 65:1899–1905.

Tang, J. X., and P. A. Janmey. 1996. The polyelectric nature of f-actin and the mechanism of actin bundle formation. *J. Biol. Chem.* 271: 8556–8563.

Unger, E., K. J. Böhm, and W. Vater. 1990. Structural diversity and dynamics of microtubules and polymorphic tubulin assemblies. *Electron Microsc. Rev.* 3:355–395.

Vater, W., W. Fritzsche, A. Schaper, K. J. Böhm, E. Unger, and T. M. Jovin. 1995. Scanning force microscopy of microtubules and polymorphic tubulin assembles in air and liquid. *J. Cell Sci.* 108:1063–1069.

Wachsstock, D. H., W. H. Schwarz, and T. D. Pollard. 1993. Affinity of α-actinin for actin determines the structure and mechanical properties of actin filament gels. *Biophys. J.* 65:205–214.

Xu, J., D. Wirtz, and T. D. Pollard. 1998. Dynamic cross-linking by α-actinin determines the mechanical properties of actin filament networks. *J. Biol. Chem.* 273:9570–9576.

Zaner, K., R. Fotland, and T. P. Stossel. 1981. Low-shear, small volume, viscoelastometer. *Rev. Sci. Instrum.* 52:85–87.

Zaner, K., and T. P. Stossel. 1983. Physical basis of the rheological properties of F-actin. *J. Biol. Chem.* 258:11004–11009.